RESEARCH ARTICLE

Astrocyte–Neuron Interaction in the Substantia Gelatinosa of the Spinal Cord Dorsal Horn via P2X7 Receptor-Mediated Release of Glutamate and Reactive Oxygen Species

Christoph Ficker,[1] Katalin Rozmer,[1] Erzsébet Kató,[2] Rómeó D. Andó,[3] Luisa Schumann,[1] Ute Krügel,[1] Heike Franke,[1] Beáta Sperlágh,[3] Thomas Riedel,[1] and Peter Illes[1]

The substantia gelatinosa (SG) of the spinal cord processes incoming painful information to ascending projection neurons. Whole-cell patch clamp recordings from SG spinal cord slices documented that in a low Ca^{2+}/no Mg^{2+} (low X^{2+}) external medium adenosine triphosphate (ATP)/dibenzoyl-ATP, Bz-ATP) caused inward current responses, much larger in amplitude than those recorded in a normal X^{2+}-containing bath medium. The effect of Bz-ATP was antagonized by the selective P2X7 receptor antagonist A-438079. Neuronal, but not astrocytic Bz-ATP currents were strongly inhibited by a combination of the ionotropic glutamate receptor antagonists AP-5 and CNQX. In fact, all neurons and some astrocytes responded to NMDA, AMPA, and muscimol with inward current, demonstrating the presence of the respective receptors. The reactive oxygen species H_2O_2 potentiated the effect of Bz-ATP at neurons but not at astrocytes. Hippocampal CA1 neurons exhibited a behavior similar to, but not identical with SG neurons. Although a combination of AP-5 and CNQX almost abolished the effect of Bz-ATP, H_2O_2 was inactive. A Bz-ATP-dependent and A-438079-antagonizable reactive oxygen species production in SG slices was proven by a microelectrode biosensor. Immunohistochemical investigations showed the colocalization of P2X7-immunoreactivity with microglial (Iba1), but not astrocytic (GFAP, S100β) or neuronal (MAP2) markers in the SG. It is concluded that SG astrocytes possess P2X7 receptors; their activation leads to the release of glutamate, which via NMDA- and AMPA receptor stimulation induces cationic current in the neighboring neurons. P2X7 receptors have a very low density under resting conditions but become functionally upregulated under pathological conditions.

GLIA 2014;00:000–000

Key words: substantia gelatinosa, astrocytes, neurons, P2X7 receptors, ATP, amino acid transmitters

Introduction

The substantia gelatinosa (SG; Layer II) of the spinal cord is an important area of sensory integration in the CNS, where incoming C and A_δ fiber axons of the primary afferents innervate local interneurons, which process nociceptive information to ascending projection neurons originating in the Layer I of the spinal cord (Furue et al., 2004; Gu and Heft, 2004). The SG receives dense descending inhibitory serotonergic and noradrenergic inputs from the raphe magnus and locus coeruleus; the afferent terminals and interneurons contain excitatory substances such as substance P and calcitonin gene-related peptide; high densities of excitatory and inhibitory interneurons in the SG utilize glutamate as excitatory and glycine/γ-aminobutyric acid (GABA) as inhibitory

View this article online at wileyonlinelibrary.com. DOI: 10.1002/glia.22707

Published online Month 00, 2014 in Wiley Online Library (wileyonlinelibrary.com). Received Jan 25, 2014, Accepted for publication May 23, 2014.

Address correspondence to Peter Illes, Rudolf-Boehm-Institute for Pharmacology and Toxicology, Haertelstrasse 16–18, Leipzig, Germany. E-mail: Peter.Illes@medizin.uni-leipzig.de

From the [1]Rudolf Boehm Institute for Pharmacology und Toxicology, University of Leipzig, Leipzig, Germany; [2]Department of Pharmacology and Pharmacotherapy, Semmelweis University, Budapest, Hungary; [3]Laboratory of Molecular Pharmacology, Institute of Experimental Medicine, Hungarian Academy of Sciences, Budapest, Hungary.

Christoph Ficker, and Katalin Rozmer contributed equally to this work.

transmitters (Brown, 1982; Furue et al., 2004). Many of these neuronal transmitters/modulators, including the endogenous nucleoside adenosine, may regulate SG functions as shown by the patch clamp technique in spinal cord slice preparations (Lao et al., 2004).

Adenosine is an active metabolite of the neuronal/glial signaling molecule adenosine triphosphate (ATP), which via various types of P2X receptors is involved in the processing and modulation of painful stimuli for example at the level of the spinal cord (Burnstock and Wood, 1996; Burnstock et al., 2011; Wirkner et al., 2007b). P2X3 receptors located at the terminals of primary sensory afferents forming synapses with dorsal horn neurons of the SG (Nakatsuka et al., 2003) facilitate the release of the neurotransmitter glutamate and hence enforce pain transmission (Gu and MacDermott, 1997). In addition, during neuropathic pain, astrocytic P2X7, and microglial P2X4/P2X7 receptors lead to the release of inflammatory mediators causing hyperalgesia and allodynia (Burnstock et al., 2011; Tsuda et al., 2005).

P2X7 receptors have originally been identified at peripheral and central immunocytes such as macrophages, lymphocytes, and microglia, where they mediate immediate necrosis and on a longer term either apoptosis or cell proliferation (Sperlágh et al., 2006). Although there is broad consensus that macroglial cells possess P2X7 receptors (Franke et al., 2012; Verkhratsky et al., 2009), there is an ongoing dispute on the question whether this receptor type is also present at peripheral and central neurons (Anderson and Nedergaard, 2006; Sim et al., 2004). The classic signaling mechanism of the P2X7 receptor channels opened by pathologically high ATP concentrations involves the sustained elevation of the intracellular-free Ca^{2+}, several second messengers, and enzyme cascades owing to the drastic change in intracellular ion homeostasis, and the release of interleukin-1β/nitric oxide (NO)/reactive oxygen species (ROS) (Skaper et al., 2010; Sperlágh et al., 2006).

The questions we attempted to answer by this study were the following: (1) Do spinal astrocytes in agreement with the supraspinal ones possess functional P2X7 receptors? (2) Do SG neurons respond to P2X7 receptor agonists directly or indirectly via signaling molecules secreted from neighboring astrocytes? (3) Does astrocytic ROS modify the sensitivity of SG neurons to P2X7 receptor agonists? We tentatively suggest that spinal astrocytes contain P2X7 receptors whose activation leads to a release of glutamate and ROS which induce and facilitate, respectively, the ensuing current responses in neurons.

Materials and Methods

Brain Slice Preparation, Whole-Cell Patch Clamp Recordings, and Drug Application Protocols

Wistar rat pups (11–14 days old) and in some cases transgenic mice expressing monomeric red fluorescent protein-1 (mRFP1) under the control of the human glial fibrillary acidic promoter (Tg(GFAP/mRFP1); 10–14 days old) were decapitated to prepare slices of their thoracolumbar spinal cord (Luo et al., 2002). The transgenic mice were a generous gift from Dr. Petra G. Hirrlinger (Paul-Flechsig-Institut für Hirnforschung, University of Leipzig) (Hirrlinger et al., 2005). All experiments were in accordance with the German guidelines for the use of animals in biomedical research. After decapitation, ventral laminectomy followed by dorsal and ventral root transection and *in situ* meninges removal was performed. The spinal cord was taken out and placed in ice-cold, oxygenated (95% O_2 + 5% CO_2) artificial cerebrospinal fluid (aCSF) of the following composition (mM): NaCl 126, KCl 2.5, $CaCl_2$ 2.4, $MgCl_2$ 1.3, NaH_2PO_4 1.2, $NaHCO_3$ 25, and glucose 11; pH 7.4. Transverse slices with a nominal thickness of 200 μm were cut from a piece of the lumbosacral spinal cord by using a vibratome (VT1200, Leica Biosystems). The slices were incubated for 30 min at 37°C in continuously aerated (95% O_2 + 5% CO_2) aCSF. A single slice was placed in a recording chamber and superfused with oxygenated aCSF at room temperature (20–24°C) at a speed of 3 mL/min. The composition of the aCSF used for superfusion was identical with that used for incubation. To create low divalent cation (low X^{2+}) conditions, $MgCl_2$ was omitted from the medium and the concentration of $CaCl_2$ was decreased to 0.5 mM.

Whole-cell patch clamp recordings were made after at least 60 min of superfusion with normal or low X^{2+} aCSF either from neurons or from astrocytes of the SG of the spinal cord. Both types of cells were visualized with an upright interference contrast microscope and 40× water immersion objective (Axioscope FS, Carl Zeiss). Astroglial cells of Tg(GFAP/mRFP1) mice were identified by means of an appropriate fluorescence filter of our microscope. Patch pipettes were produced by a horizontal micropipette puller (P-97, Sutter Instruments) from borosilicate capillaries. They were filled with intracellular solution of the following composition (mM): K-gluconic acid 140, $MgCl_2$ 1, HEPES 10, EGTA 11, Mg-ATP 1.5, Li-GTP 0.3, and Lucifer Yellow (LY) 0.1; pH 7.3. Pipette resistances were in the range of 5–7 MΩ.

The SG was clearly discernible as a relatively translucent band across the dorsal horn, somewhat below the surface of the spinal cord (Fig. 1Aa). After being filled with LY, fluorescence microscopy showed that neurons had round and sharply edged contours (Fig. 1Ab, upper panel), whereas astrocytes possessed many bushy processes (Fig. 1Ab, lower panel). As both cell types were of similar shape and size (diameter, ~7 μm), under our recording conditions, neurons could be discriminated from astrocytes only by their abilities to fire action potentials in the current–clamp recording mode of the patch clamp amplifier (Multiclamp 700A, Molecular Devices). For this purpose hyper- and depolarizing current pulses of increasing amplitude (50–150 pA, depending on the membrane resistance) were injected into the respective cells.

The resting membrane potential (V_m) of the astrocytes was somewhat higher than that of the neurons. When the liquid junction potential of −15.2 mV (calculated V_{LJ} between the bath and the pipette solutions; Wirkner et al., 2007a) was used for correction, V_m of a population of SG astrocytes and neurons was −86.4 ± 3.7 mV ($n = 56$) and −69.7 ± 2.1 mV ($n = 38$), respectively. The membrane resistance (R_m) of the astrocytes and neurons in the same population

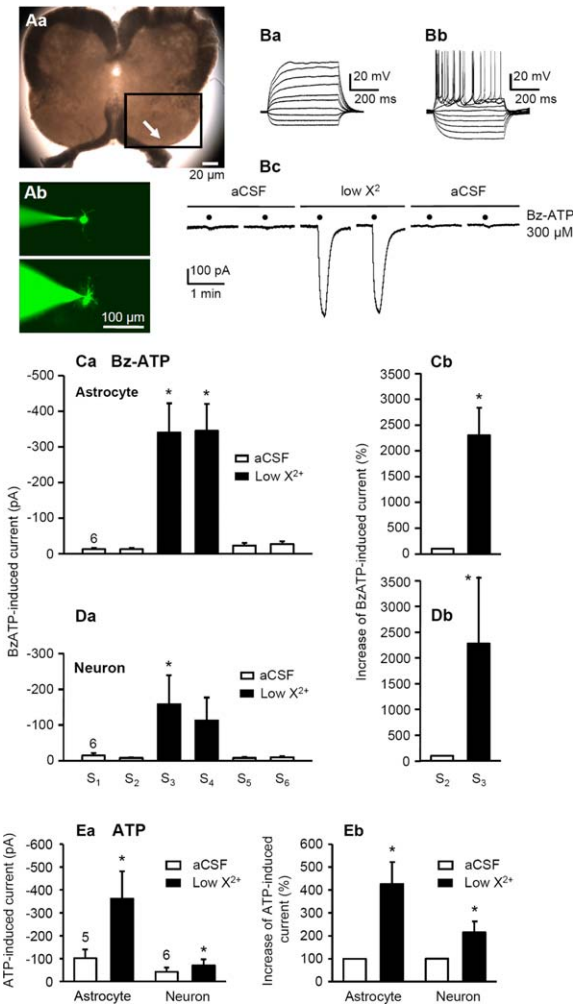

FIGURE 1: Visual and electrophysiological identification of neurons and astrocytes in the SG of the thoracolumbar spinal cord; increase of Bz-ATP-induced currents in a low X^{2+} external medium. A: Fluorescence/light microscopic image of a horizontal section of the spinal cord. White arrow points to the SG (layer II) just below the superficial layer I (a). The framed part of a is shown at a higher magnification in b. An astrocyte filled with LY diffusing from the intracellular solution for 15 min via the patch clamp pipette (left blurred cone) is shown under ultraviolet light illumination. The diffusion of LY is confined to a single cell excluding the existence of syntitial multicellular astrocytic structures. Whole-cell patch clamp measurements were used. B: Series of hyper- and depolarizing current pulses were supplied to measure whether the patched cell reacts with an action potential. Typical electrotonic voltage responses of an astroglial cell to current injection (a). Action potential firing of a neuron after injection of depolarizing current pulses above a certain threshold voltage (b). At a holding potential of −80 mV, Bz-ATP (300 µM) was applied six times (S_1–S_6) as described in the Methods section (c). C, D: Reversible increase of the Bz-ATP (300 µM) current amplitude by a low X^{2+} external medium both in astrocytes (C) and in neurons (D). The holding potential was −80 mV for astrocytes and −70 mV for neurons both in this and all subsequent experiments throughout. Absolute current amplitudes (a) and percentage increase of the current from S_2 to S_3 (b). E: A low X^{2+} aCSF potentiated the ATP (3 mM)-induced current both at astrocytes and at neurons. Absolute current amplitudes (a) and percentage increase of the current from S_2 to S_3 (b). Mean ± S.E.M of six experiments each in (C–E). *$P < 0.05$; statistically significant differences from S_2. The number of experiments is indicated in each panel.

was 290.0 ± 47.5 and 699.2 ± 75.1 MΩ, respectively. The rather high R_m values indicate that both cell types were small and astrocytes were probably not or only to a minor extent interconnected by low-resistance pathways. Then, the holding potentials of the astrocytes (−80 mV) and neurons (−70 mV) were set near to their resting membrane potential values in the voltage–clamp recording mode of the amplifier. A voltage-step protocol in the range of −80 to +30 mV for neurons and in the range of −160 to +60 mV for astroglial cells was used. Step duration was 500 ms, and the steps were delivered with an interval of 2 s. Cells where the series resistance (R_s) varied more than 20% during the experiments were discarded; there was no compensation for the R_s before recording was started.

Multiclamp and pClamp software (Molecular Devices) were continuously used to store the recorded data to perform offline analysis/filtering and to trigger the application system used. All compounds were pressure injected locally by means of a computer-controlled DAD12 superfusion system (Adams and List). The drug application tip touched the surface of the brain slice and was placed 100–150 µm from the patched cell. Agonists were applied every 5 min for 10 s each, either at increasing (Fig. 2Aa,b) or at stable concentrations (Fig. 1Bc,Ca,Da). When the interaction of 2′(3′)-*O*-(4-benzoylbenzoyl)adenosine-5′-triphosphate tri(triethylammonium) salt (Bz-ATP) with excitatory amino acid (EAA), $GABA_A$, or P2X7 receptor antagonists was studied, a stable concentration of Bz-ATP was applied with the usual protocol before (S_1, S_2), during (S_3, S_4), and after superfusion (S_5, S_6) with these antagonists for 10 min (Fig. 3A–G). When the interaction of Bz-ATP with H_2O_2, *N*-acetyl-L-cysteine (NAC) and catalase was studied, Bz-ATP was applied with a slightly modified protocol before, during, and after superfusion with the ROS modulators (Fig. 5A–D). H_2O_2, NAC, or catalase was applied 5 min after the first application of Bz-ATP (at S_2), and was left in the superfusion medium for 10 min in total. Thus, 10 min elapsed between the first and the second Bz-ATP injection (S_1, S_3), whereas only 5 min elapsed between the second and third Bz-ATP injection (S_3, S_4). Eventually, the protocol used to study the facilitation of Bz-ATP or ATP effects by a low X^{2+} medium differed from the above standard procedure in that low X^{2+} was superfused for 10 min after S_2 before the P2X7 receptor agonists were applied at S_3 for 10 s. Excised patches were prepared by slowly withdrawing the pipette and hence separating the patch from the surrounding cells.

In some of the experiments, hippocampal slices of rats were prepared by the procedures described earlier (Leichsenring et al., 2013). Whole-cell patch clamp recordings were made either from neurons of the CA1 region, or astrocytes from the oriens region in close apposition to CA1 (distance, ∼200 µm). Compositions of the extra- and intracellular media were identical with those used for SG neurons and astrocytes. All further experimental conditions including cell-type identification, recording arrangements, drug application protocols, and evaluation procedures were also similar.

Biosensor Measurements of ROS

In brief, 300-µm-thick coronal sections of the lumbosacral spinal cord were cut by using a vibratome. Tissue slices were stored in low X^{2+} aCSF under constant aeration with a mixture of 95% O_2 and 5% CO_2 for at least 45 min and then transferred to the slice

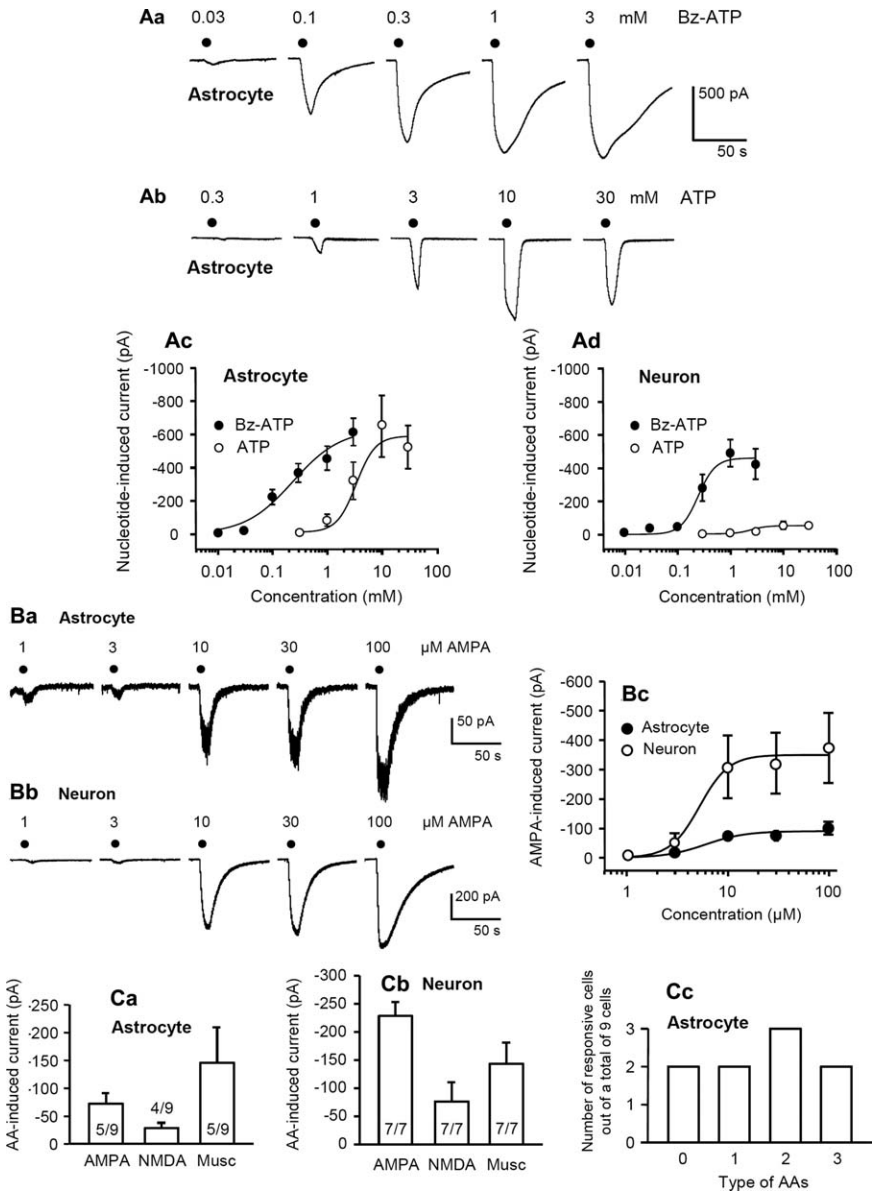

FIGURE 2: Comparison of the effects of ATP and Bz-ATP on neurons and astrocytes in the SG of the thoracolumbar spinal cord; effects of excitatory and inhibitory amino acid transmitters. Whole-cell patch clamp measurements were used. A: Concentration–response relationship for Bz-ATP (a) and ATP (b) in astrocytes at the indicated concentrations in a low X^{2+} aCSF; representative recordings. The experimental protocol is described in the Methods section. Plot of increasing logarithmic concentrations of AMPA against the nucleotide induced current, both for astrocytes (c) and for neurons (d). It is noteworthy that in comparison with Bz-ATP, the concentration–response curve of ATP was shallower and exhibited a lower maximum at neurons. The calculated parameters of the curves were as follows: astrocytes (Bz-ATP, $EC_{50} = 237.5 \pm 110.9$ μM, $E_{max} = 631.2 \pm 93.1$ pA, $n = 10$; ATP, $EC_{50} = 2{,}635.2 \pm 632.3$ μM, $E_{max} = 591.6 \pm 65.9$ pA, $n = 10$), neurons (Bz-ATP, $EC_{50} = 247.4 \pm 36.6$ μM, $E_{max} = 457.1 \pm 30.7$ pA, $n = 7$; ATP, $EC_{50} = 5{,}968.0 \pm 1{,}790.8$ μM, $E_{max} = 58.7 \pm 4.3$ pA, $n = 4$). B, C: Effects of AMPA, NMDA, and muscimol on neurons and astrocytes in the SG at a low X^{2+} external medium. B: Concentration–response relationship for AMPA. Representative recordings from astrocytes (a) and neurons (b). The experimental protocol is described in the Methods section. Plot of increasing logarithmic concentrations of AMPA against the nucleotide induced current in both cell types (c). The calculated parameters of the concentration–response curve for AMPA were as follows: astrocytes ($EC_{50} = 5.9 \pm 2.2$ μM, $E_{max} = 90.7 \pm 12.0$, $n = 7$), neurons ($EC_{50} = 5.3 \pm 0.9$ μM, $E_{max} = 349.9 \pm 19.6$ pA, $n = 5$). C: Current responses to AMPA, NMDA, and muscimol at 100 μM each, in neurons (a) and astrocytes (b). Mean ± S.E.M. of the responsive cells out of the total cells of nine investigated (as indicated in the columns). The experimental protocol is described in the Methods section. AA, amino acid transmitters. The number of responsive cells is shown for the astrocytes (c). It is noteworthy that some cells did not react to any of the AA transmitters, whereas other ones reacted to 1, 2, or even all 3 transmitters.

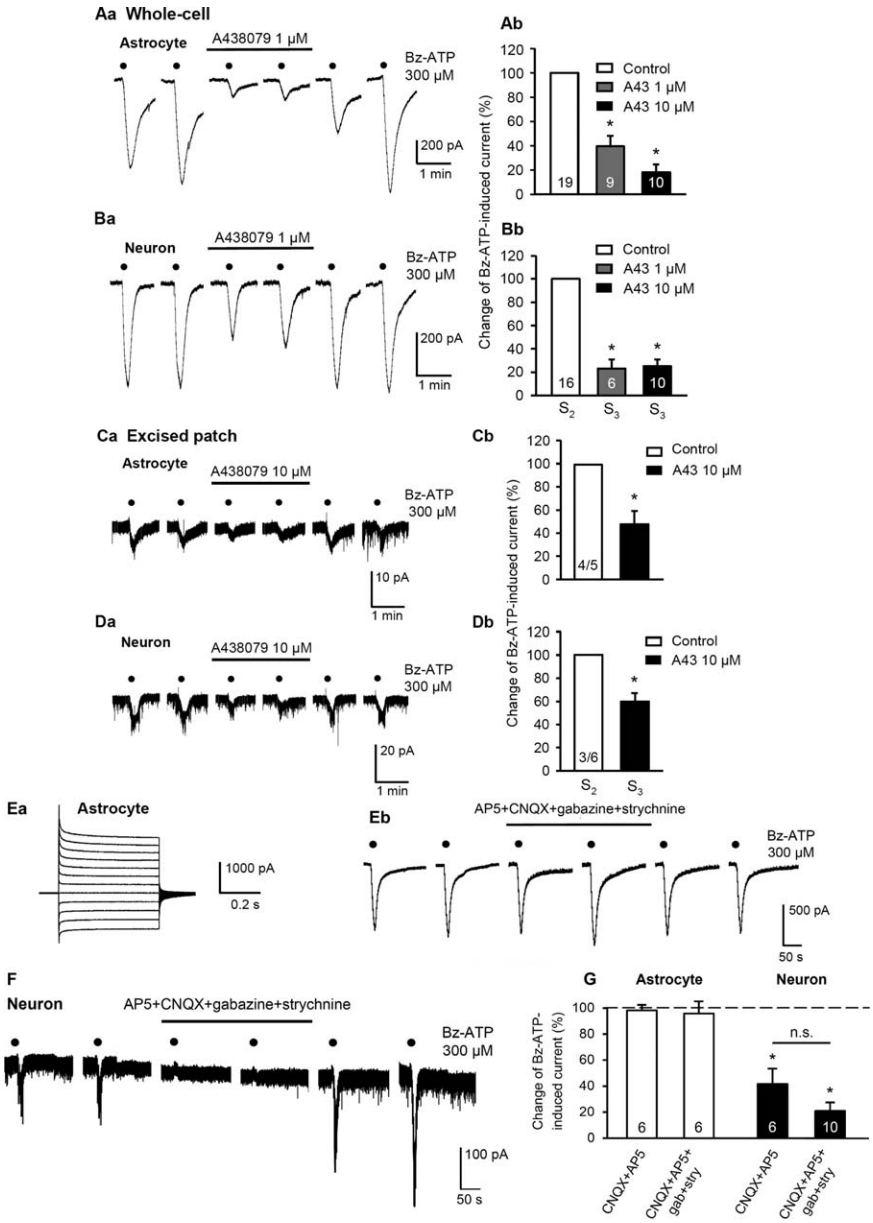

FIGURE 3: Inhibition of Bz-ATP induced currents by A-438079 both in neurons and in astrocytes of the SG in a low X^{2+} external medium; blockade of Bz-ATP effects by excitatory and inhibitory amino acid (AA) receptor antagonists in neurons but not astrocytes. Whole-cell patch clamp measurements were used in (A, B) and excised patches were prepared in (C, D). Bz-ATP was applied six times (S_1–S_6) as documented by the original tracings and according to the protocol described in the Methods section. A: Depression by A-438079 (1 μM) of the Bz-ATP (300 μM)-induced current in astrocytes. Representative recording in one cell (a). Concentration-dependent inhibition of the Bz-ATP (300 μM)-induced current by A-438079 (1, 10 μM; b). Percentage mean ± S.E.M. change of the current amplitude from S_2 to S_3 at the indicated number of cells. B: Depression by A-438079 (1 μM) of the Bz-ATP (300 μM)-induced current in neurons. Representative recording in one cell (a). Concentration-dependent inhibition of the Bz-ATP (300 μM)-induced current by A-438970 (1, 10 μM; b). Percentage mean ± S.E.M. change of the current amplitude from S_2 to S_3 at the indicated number of cells. C, D: Excised patch experiments in astrocytes (C) and neurons (D) similar to those made under whole-cell conditions. Representative recordings in one cell (a) and percentage mean ± S.E.M. change in the current amplitude from S_2 to S_3 at the indicated number of cells (b). All excised astrocytic patches responded to Bz-ATP, but only four out of the five astrocytes and only three out of the six neurons exhibited A-438079-sensitivity. *$P<0.05$; statistically significant difference from the control current at S_2. E–G: Inhibition of Bz-ATP effects by excitatory and inhibitory amino acid (AA) receptor antagonists in neurons but not astrocytes. Voltage/current characteristics of an astrocyte generated by voltage steps from −160 to +60 mV in 20 mV increments from a holding potential of −80 mV (Ea). Combination of excitatory (AP-5, 50 μM; CNQX, 20 μM) and inhibitory (gabazine, strychnine, 10 μM each) (AA) receptor antagonists did not alter the Bz-ATP (300 μM) currents in astrocytes (Eb), but inhibited them in neurons (F). Representative recordings. G: Mean ± S.E.M. of the indicated number of experiments performed in a similar manner as described for E and F. *$P<0.05$; statistically significant difference from the control current at S_2. n.s.; no statistical significant difference between the two columns.

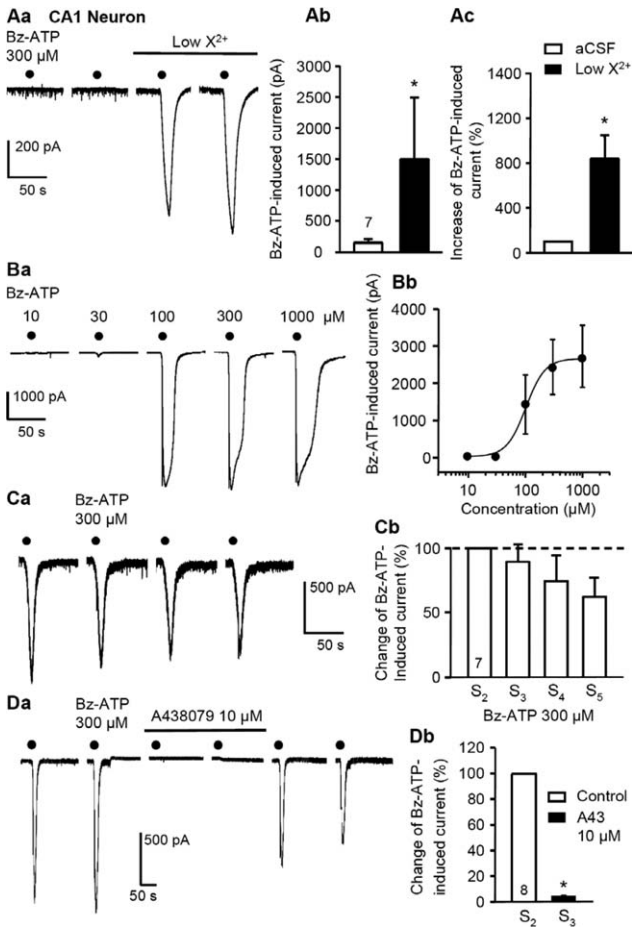

FIGURE 4: Effect of Bz-ATP on hippocampal CA1 pyramidal cells and interaction with A-438079. Whole-cell patch clamp measurements were used. The holding potential was −70 mV in this figure and also in the next one. The same concentration (300 μM) of Bz-ATP was applied four to six times (S_1–S_6; A, C, D) or increasing concentrations of this drug (10–1,000 μM) were applied to construct concentration–response relationships (B) as documented by the original tracings and according to the protocols described in the Methods section. A: Increase of the Bz-ATP (300 μM)-induced current amplitude by a low X^{2+} external medium. Representative recording (a). Absolute current amplitudes (b) and percentage increase of the current from S_2 to S_3 (c). Mean ± S.E.M. of seven experiments. *$P<0.05$; statistically significant differences from S_2. B: Concentration–response relationship for Bz-ATP in a low X^{2+} external medium. Representative recording (a) and plot of increasing logarithmic concentrations of Bz-ATP against the nucleotide-induced current (b). Mean ± S.E.M. of the current amplitudes in five experiments. The calculated parameters of the concentration–response curve for Bz-ATP were as follows: $EC_{50} = 96.0 \pm 6.5$ μM, $E_{max} = 2{,}658.2 \pm 95.2$ pA, $n = 5$). C: Reproducibility of the Bz-ATP (300 μM) current amplitudes during four applications (S_2–S_5; S_1 discarded). Representative experiment (a) and percentage change with respect to S_2 (b). There was no statistically significant difference between the individual current amplitudes. D: A-438079 (10 μM) abolishes the Bz-ATP (300 μM)-induced current. Representative experiment (a) and percentage change with respect to S_2 (b). *$P<0.05$; statistically significant difference from S_2. Mean ± S.E.M. of the indicated number of experiments in Cb and Db.

chamber for measurement, with constant perfusion of standard aCSF at a speed of 3 mL/min. After transferring spinal cord slices to the flow chamber, biosensors were gently inserted into the tissue at the SG close to each other. After 5 min of equilibration, electrochemical recordings were started. Biosensor microelectrode measurements were carried out similarly as to the previously published methods (Heinrich et al., 2012) using ROS and NULL Pt/Ir microelectrode biosensors (sarissaprobes®, Sarissa Biomedical) with sensing tips of 50 μm in diameter and 0.5 mm in length. The surface of the ROS biosensors was deposited with superoxide dismutase and catalase enzymes to break down ROS and served as interference controls to NULL sensors, which lacked these reductive enzymes. The net signal difference (NULL − ROS) was calculated and calibration curves (Fig. 6A) were used to obtain the relevant concentrations of *in situ* ROS.

Bz-ATP (300 μM) was superfused for 2 min. When applied, the P2X7 antagonist A-438079 (10 μM) was preperfused for 10 min before BzATP stimulation. Using the calibration curve constructed from the net signal of known H_2O_2 concentrations ranging from 1 to 10 μM (Fig. 6A, inset), the maximal increases evoked by the drug treatments were read of at their peaks and were expressed in H_2O_2 (μM) equivalents. In two out of the eight slices (BzATP) and one out of the six slices (BzATP plus A-438079), the treatments did not evoke detectable ROS release (no increase in net signal compared with baseline, and therefore yielding negative maximal values); these values were not included in the analysis.

Immunofluorescence and Confocal Microscopy

Rats were transcardially perfused under anesthesia with paraformaldehyde (2%) in sodium acetate buffer (pH 6.5; Solution A) followed by paraformaldehyde (2%) in sodium borate buffer (pH 8.5; Solution B) (Franke et al., 2004). Then, the brains were removed, stored overnight in Solution B, and 50 μm coronal sections of their hippocampal formation, and the spinal cord containing the SG was prepared using a vibratome (Leica Biosystems). In some cases, spinal cord slices (thickness, 100 μm), kept in oxygenated aCSF for 2–3 h, similar to those used for electrophysiological recordings, were processed for immunohistochemical investigations.

In brief, 50-μm-thick brain slices from transcardially perfused brains were incubated with antibody mixtures of rabbit anti-P2X7 (1:600; Alomone Labs) and/or with mouse anti-GFAP (1:1,000; glial fibrillary acidic protein; Santa Cruz), or mouse anti-S100β (1:600; S100 Protein Ab-1, Clone 4C4.9; Dianova), mouse anti-MAP2 (1:1,000; microtubule associated protein; Chemicon), as well as goat anti-Iba1 (1:50; goat polyclonal to Iba1; Abcam) together with 0.3% Triton X-100 and 5% fetal calf serum (FCS) in Tris-buffered saline (TBS) for 48 h at 4°C.

For the simultaneous visualization of the different primary antibodies, mixtures of secondary antibodies specific for the appropriate species IgG (rabbit, mouse, and goat) were applied. Carbocyanine (Cy)2- (1:400), Cy3- (1:1,000), Cy5- (1:100)-conjugated IgGs (all from Jackson ImmunoResearch) diluted in 0.3% Triton X-100 and 5% FCS in TBS were applied, respectively, for 2 h at room temperature. Control experiments were performed without all primary antibodies or by preadsorption of the antibody with the immunizing peptides. After mounting on glass slides, all stained sections

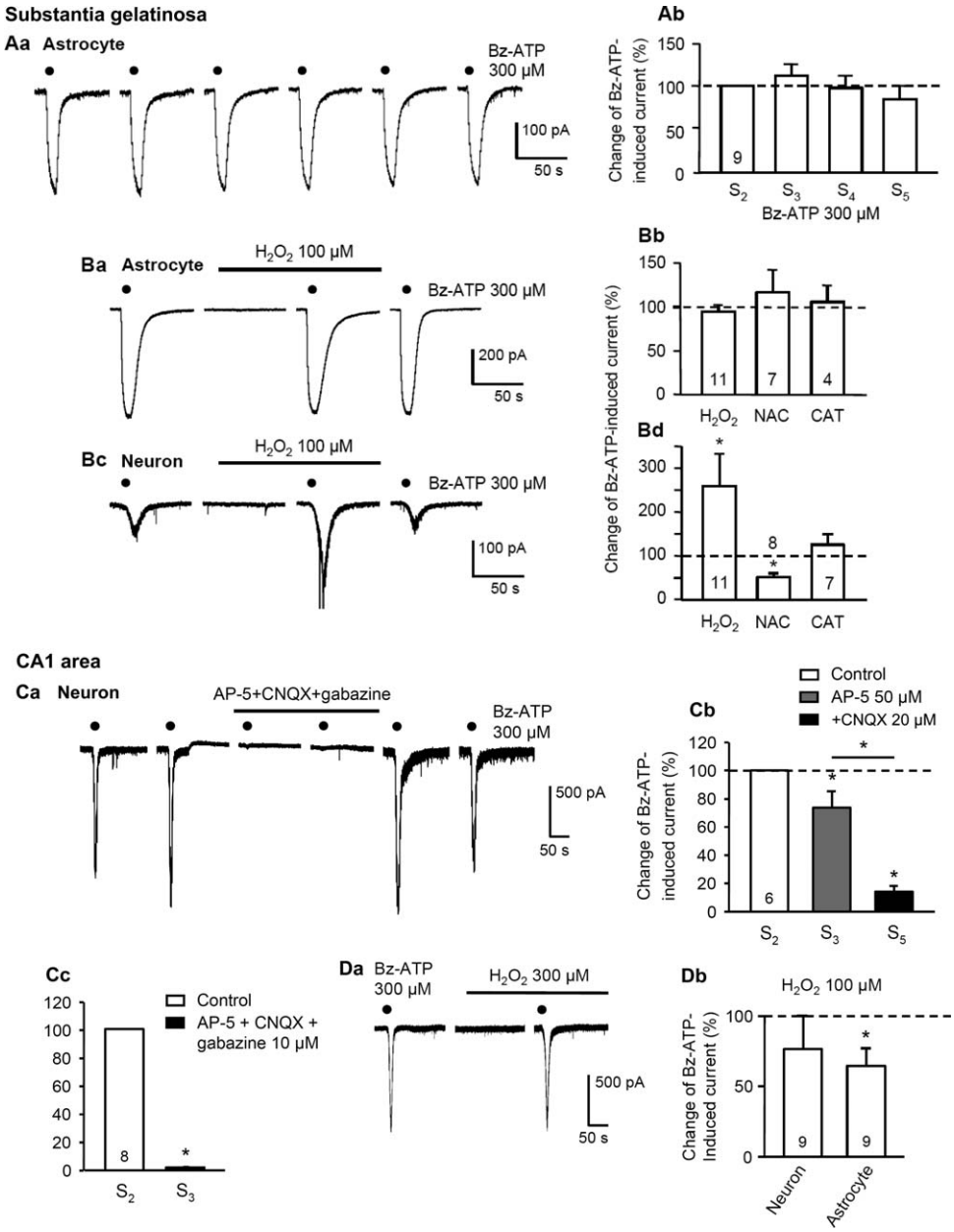

FIGURE 5: Modulation of Bz-ATP-induced currents by H_2O_2 and its scavengers in neurons and astrocytes of the SG, and in neurons of the hippocampal CA1 area in a low X^{2+} external medium; blockade of Bz-ATP effects in CA1 neurons by excitatory and inhibitory amino acid (AA) receptor antagonists. Whole-cell patch clamp measurements were used. A: Repetitive application of Bz-ATP (300 μM) causes stable current amplitudes in SG astrocytes. Representative experiment (a) and percentage mean ± S.E.M. change in the current amplitude from S_2 to S_5 at the indicated number of cells (b). There was no statistically significant difference between the currents between S_2 and S_5. B: Effects of H_2O_2 (100 μM), NAC (10 mM), and catalase (CAT; 1,000 U/mL) on the astrocytic and neuronal Bz-ATP (300 μM)-induced currents. Representative recordings demonstrate that H_2O_2 did not alter the effect of Bz-ATP in astrocytes (a), but facilitated it in neurons (c). There was no effect of H_2O_2 by its own on either cell type. Percentage mean ± S.E.M. change of the current amplitude from S_2 to S_3 by H_2O_2, NAC, and CAT at the indicated number of astrocytes (b) or neurons (d). *$P<0.05$; statistically significant difference from S_2. C: Combination of excitatory (AP-5, 50 μM; CNQX, 20 μM) and inhibitory (gabazine, 10 μM) AA receptor antagonists abolished the Bz-ATP (300 μM) currents in CA1 hippocampal neurons. Representative recording (a). Mean ± S.E.M. of the indicated number of experiments carried out during the sequential application of AP-5 (50 μM) and AP-5 plus CNQX (20 μM) (b) or AP-5, CNQX, and gabazine (10 μM) together (c). D: H_2O_2 (300 μM) failed to alter the effect of Bz-ATP (300 μM) in neurons, but depressed it in astrocytes. Representative recording (a). Mean ± S.E.M. of the indicated number of experiments for neurons and astrocytes (b). *$P<0.05$; statistically significant difference from the current at S_2.

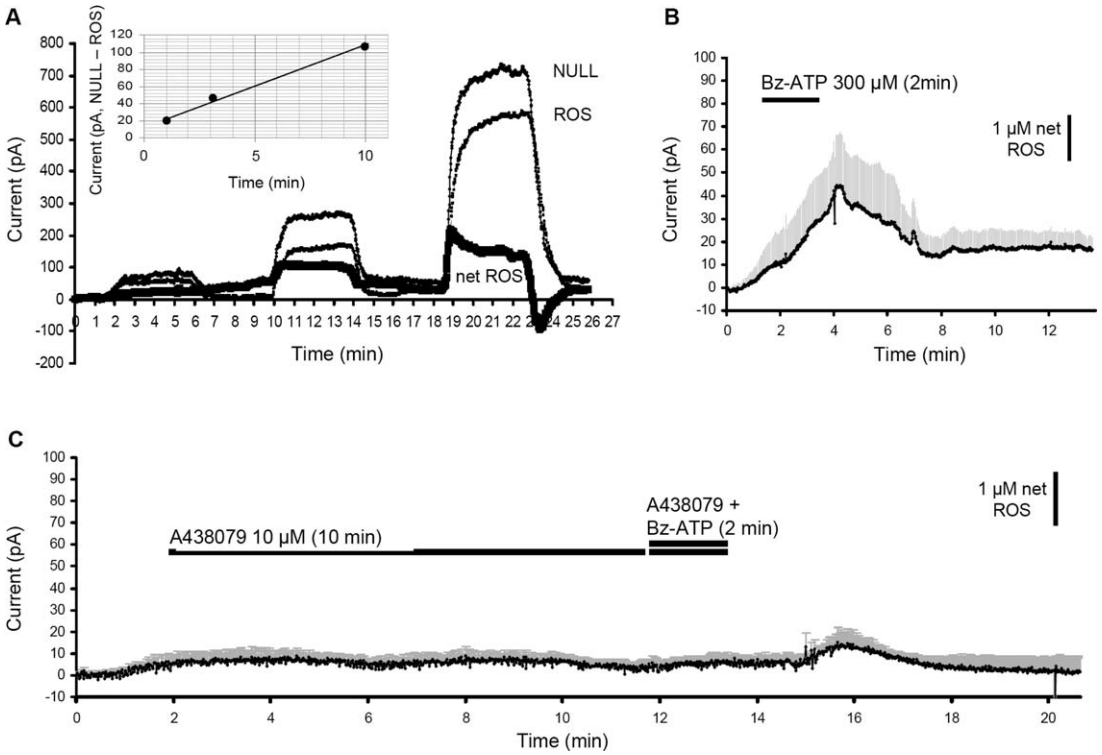

FIGURE 6: Biosensor measurement of the production/release of ROS in rat SG slices. A: Calibration curve and ROS biosensor traces showing responses to H_2O_2 (0.1–10 μM, net signal = ROS NULL, bottom). B: BzATP (300 μM, 2 min) induced ROS release. Black trace denotes the average of net signals, whereas gray bars show S.E.M. (values in pA; $n = 6$; average of peak values correspond to 7.07 ± 1.99 μM ROS). C: Antagonistic effects of the P2X7 antagonist A-438079 (10 μM, 10 min) on BzATP-induced increase of ROS in the SG. Black trace denotes the average of net signals, whereas gray bars above show S.E.M. (values in pA; $n = 5$; average of peak values correspond to 1.30 ± 0.57 μM ROS). A-438079 did not alter the ROS release but antagonized the effect of Bz-ATP.

were dehydrated in a series of graded ethanol, processed through *n*-butyl acetate and coverslipped with Entellan (Merck).

The double and triple immunofluorescences were investigated by a confocal laser scanning microscope (LSM 510 Meta, Carl Zeiss) using excitation wavelengths of 633 nm (helium/neon2, blue Cy5-labelling), 543 nm (helium/neon1, red Cy3-immunofluorescence), and 488 nm (argon, yellow-green Cy2-immunofluorescence).

Materials

The following drugs were used: adenosine 5′-triphosphate disodium salt hydrate (ATP), catalase from bovine liver, hydrogen peroxyde (H_2O_2), *N*-acetyl-L-cysteine (NAC), *N*-methyl-D-aspartic acid (NMDA), strychnine hydrochloride (Sigma-Aldrich); (S)-α-amino-3-hydroxy-5-methyl-4-isoxazolepropionic acid (S-AMPA), 2′(3′)-*O*-(4-benzoylbenzoyl)adenosine-5′-triphosphate tri(triethylammonium) salt (Bz-ATP), 3-[[5-(2,3-dichlorophenyl)-1*H*-tetrazol-1-yl]methyl]pyridine hydrochloride (A-438079), 6-cyano-7-nitroquinoxaline-2,3-dione, D-(−)-2-amino-5-phosphonopentanoic acid, gabazine, muscimol (Tocris Bioscience). The pH value of the ATP-containing aCSF superfused onto the neurons/astrocytes was adjusted by NaOH to 7.4.

Statistics

Concentration–response curves for agonists were fitted by using a three parametric Hill plot (SigmaPlot 11.0; SPSS). Means ± S.E.M. are given throughout. SigmaPlot 11.0 was used for statistical evaluation. Multiple comparisons between data were performed by one-way analysis of variance (ANOVA) followed by the Holm–Sidak test. Two data sets were compared by using the Student's *t*-test or the Mann–Whitney rank sum test as appropriate. In all cases, a probability level of 0.05 or less was considered to be statistically significant.

Results

Current Responses Induced by Bz-ATP/ATP, Glutamate, and GABA in Astrocytes and Neurons of the Rat Spinal Cord SG; Mediation of ATP Effects by P2X7 Receptors

Initially, the cell type recorded from (astrocyte or neuron) was identified. There was no discrimination between the different astrocytes described, for example, for the prefrontal cortex or the hippocampal oriens layer (outwardly rectifying, variably rectifying, passive; classification based on the current/voltage characteristics; Leichsenring et al., 2013; Oliveira et al., 2011), which were also present in the SG. In addition, we did not characterize the various types of neurons described for the SG (phasic, tonic, irregular, delay, transient;

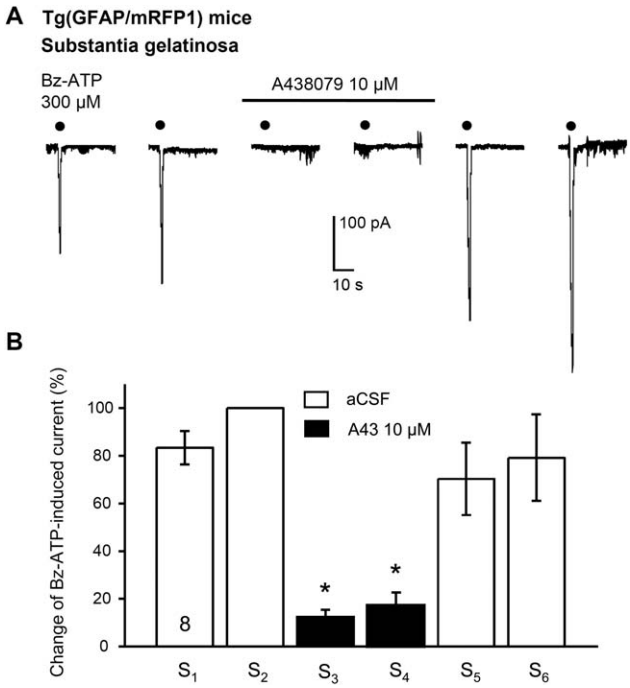

FIGURE 7: Inhibition of Bz-ATP-induced currents by A-438079 in astrocytes of the SG in a low X^{2+} external medium; Tg(GFAP/mRFP1) mice were used in these series of experiments. Whole-cell patch clamp measurements at a holding potential of −80 mV. Bz-ATP was applied six times (S_1–S_6) as documented by the original tracings and according to the protocol described in the Methods section. A: Depression by A-438079 (10 μM) of the Bz-ATP (300 μM)-induced current in astrocytes. Representative recording in one cell. B: Inhibition of the Bz-ATP (300 μM)-induced current by A-438079 (10 μM). Percentage mean ± S.E.M. change of the current amplitude from S_2 to S_3 and S_4 at eight cells. The effect of A-438079 was reversible on washout. The amplitude of the Bz-ATP-induced current at S_2 was 109.4 ± 23.0 pA ($n = 8$). *$P < 0.05$; statistically significant differences from S_2 (100%).

classification on the basis of the firing pattern and morphological properties; Grudt and Perl, 2002).

It was an important point to decide whether recordings are from astrocytes or from microglia. Microglial cells in brain slices may exhibit morphological characteristics somewhat similar to astroglia after LY filling and also fail to fire action potentials in response to depolarizing current injection (Fig. 1Ab, lower panel; compare Fig. 1Ba with Bb) (Boucsein et al., 2000). However, in voltage–clamp recordings, resting microglia express a typical inwardly rectifying current pattern and acquire an additional outwardly rectifying current component only after cell activation, for example, after facial nerve axotomy (Boucsein et al., 2000), status epilepticus (Ulmann et al., 2013), or probably also the preparation of brain slices from living tissue (Fig. 8Cci). The astrocytes we recorded exhibited voltage–current characteristics clearly differing from those of the resting or activated microglia.

Then, we compared the Bz-ATP sensitivity of rat SG neurons and astrocytes. At a holding potential of −80 mV, SG astrocytes responded to Bz-ATP (300 μM) in the standard aCSF with only very small current responses (Fig. 1Bc,Ca,b). However, when the concentration of divalent cations was reduced or even abolished (0.5 mM Ca^{2+}/no Mg^{2+}; low X^{2+} medium), the effect of Bz-ATP markedly increased. Two subsequent applications of Bz-ATP (300 μM) caused reproducible current responses, both in a normal and in a low X^{2+} medium. In addition, the potentiation induced by the lack of divalent cations rapidly reversed after returning to normal X^{2+} conditions. We evaluated both the absolute current amplitudes before, during, and after superfusion with low X^{2+} aCSF (Fig. 1Ca) and the percentage increase of the Bz-ATP effects from S_2 to S_3 (Fig. 1Cb).

Similar results were obtained for SG neurons although in this series of experiments the second application of Bz-ATP (300 μM; S_4) in the presence of a low X^{2+} medium caused less current than its first application (S_3; Fig. 1Da). Nevertheless, the percentage increase of the Bz-ATP effect by a low X^{2+} external solution was comparable for astrocytes (to 2,304.3 ± 526.4%; $n = 6$; $P < 0.05$ from 0%) and neurons (to 2,279.2 ± 1,286.8%; $n = 6$; $P < 0.05$ from 0%) (Fig. 1Cb,Db). It is noteworthy that both the Bz-ATP current amplitudes at low Ca^{2+}/no Mg^{2+} and their percentage increase under these conditions strongly varied between the individual neurons, giving rise to considerable scatter around the means.

It is necessary to repeatedly point out that in contrast to SG astrocytes, SG neurons form a very inhomogenous population. The majority of SG neurons are excitatory, whereas their inhibitory counterparts represent a minority (Landry et al., 2004; Santos et al., 2007). It was also reported that supposedly glutamatergic, excitatory SG neurons are presynaptically inhibited by opioid μ-receptor agonists, whereas the inhibitory ones are opioid resistant (Santos et al., 2004). In contrast, purinergic P2X7 receptor agonists indiscriminately activated SG neurons, irrespective of their firing patterns (this study). However, differences in receptor sensitivities may explain the large scatter in the current amplitudes.

Then, we tested the effect of the mother compound of Bz-ATP, ATP itself. Once again, ATP (3 mM) produced only small current responses in astrocytes and neurons in a normal aCSF, which, however, largely increased in the presence of a low X^{2+} medium (Fig. 1Ea,b). In agreement with the Bz-ATP experiments, the low X^{2+} extracellular solution appeared to cause a weaker potentiation of the ATP-induced currents in neurons (to 214.2 ± 48.1%; $n = 6$; $P < 0.05$ from 0%) than in astrocytes (to 426.4 ± 95.4%; $n = 5$; $P < 0.05$ from 0%) although this difference did not reach the level of statistical significance (Fig. 1Eb).

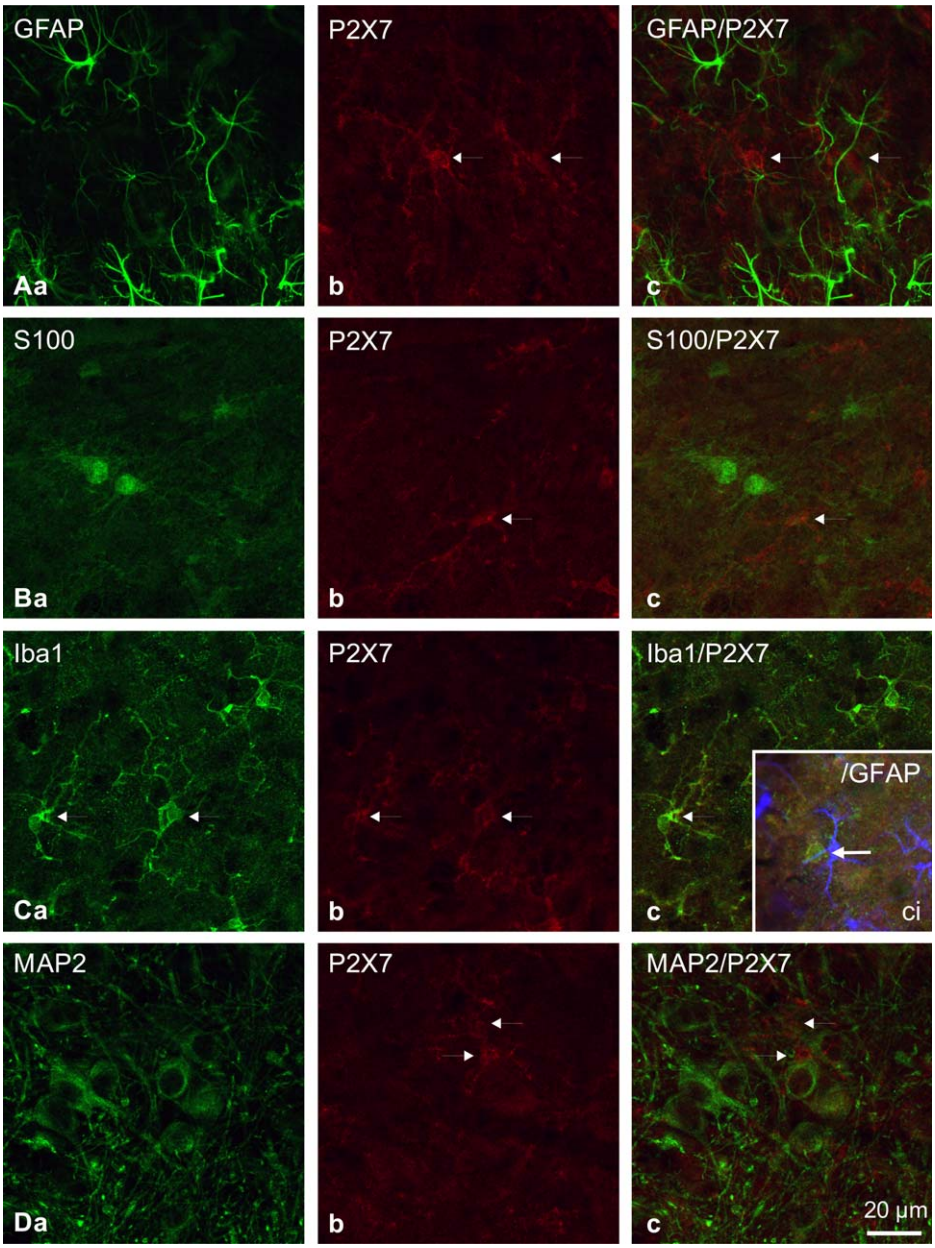

FIGURE 8: Confocal images of multiple immunofluorescence labeling of rat SG slices. Rats were either killed after perfusion fixation by decapitation, and their brains were immediately processed for immunohistochemistry, or brain slices were at first incubated in aCSF for 2–3 h to imitate electrophysiological recording conditions, and immunohistochemistry procedures were only applied thereafter (Cci). No colocalization of glial fibrillary acidic protein- (GFAP; astrocytes; (A), S100β- (S100; astrocytes; (B) and microtubule-associated protein-2- (MAP-2; neurons; (D) IR with P2X7 receptor-IR was observed. In contrast, Iba1-IR (microglia) clearly colocalized with P2X7 (C). Comparison of Cci with Cc shows that the double staining for Iba1/P2X7 persists during conditions which imitate electrophysiological recordings. However, microglial cells lost their numerous cellular processes, indicating activation by the preparation procedure. We used a homogenous color coding in (A–D) and a separate one in Cci. (A–D): GFAP, S100, Iba1, MAP2 (green), P2X7 (red); Cci: Iba1 (green), P2X7 (red), GFAP (blue). Thin arrows indicate the P2X7-IR throughout. Scale bars for all panels, 20 μm.

In all subsequent experiments, a low X^{2+} extracellular medium was used throughout. Increasing concentrations of Bz-ATP (0.03–3 mM) and ATP (0.3–30 mM) (Fig. 2Aa,b) induced inward currents; the plots of the logarithmic agonist concentrations against the current amplitudes yielded the concentration–response curves shown in Fig. 2Ac,d. Both at astrocytes and at neurons, Bz-ATP was much more potent than ATP itself. In addition, the maximum current amplitudes for ATP and Bz-ATP were similar at the astrocytes, but not at the neurons. The concentration–response curve of ATP at the neurons was much more shallow and reached only a lower maximum than the comparable curve for Bz-

ATP did (for the respective EC_{50} and E_{max} values; see the legend of Fig. 2Ac,d).

As ATP is an early neural signaling molecule, we investigated the effects of prototypic excitatory and inhibitory transmitters in SG neurons and astrocytes. AMPA and NMDA were used to stimulate the respective ionotropic glutamate receptors, whereas muscimol was used to activate the $GABA_A$ receptor channel. AMPA (1–100 μM) elicited astrocytic/neuronal currents of amplitudes depending on the agonist concentration (Fig. 2Ba–c). It was absolutely clear that the size of the neuronal currents markedly surmounted that of the astrocytic ones (for the IC_{50} and E_{max} values; see the legend of Fig. 2Bc). In addition, a near maximum was reached already at 10 μM AMPA, without a further relevant change up to 100 μM. In separate experiments, 100 μM of AMPA, NMDA, and muscimol were tested on the same astrocyte or neuron (Fig. 2Ca–c). The larger AMPA responses at neurons in comparison with astrocytes could also be confirmed under these conditions and in addition NMDA exhibited the same neuron/astrocyte activity ratio as AMPA (Fig. 2Ca,b). In spite of using a Mg^{2+}-free (and low Ca^{2+}) medium, which relieves the Mg^{2+} block of the NMDA receptor channel, NMDA was on both cell types less active than AMPA. In contrast to the excitatory amino acid agonists, muscimol caused similar current amplitudes at neurons and astrocytes. Eventually, AMPA, NMDA, and muscimol acted on all neurons investigated, but only at a subpopulation of astrocytes (Fig. 2Ca–c). Out of the total cell number of nine, two astrocytes reacted to none of the agonists, and a variably number of cells reacted to 1, 2, or 3 agonists (Fig. 2Cc). Hence, in contrast to the astrocyte preferring properties of Bz-ATP and ATP (Fig. 1B–E), all amino acid transmitters (except muscimol) preferred neurons over astrocytes. This was evident when the current amplitudes and/or the proportion of the activated cells were taken into consideration.

Then, we asked ourselves, whether Bz-ATP acts primarily at SG astrocytes (which in other regions of the CNS were repeatedly described to possess P2X7 receptors; Illes et al., 2012; Oliveira et al., 2011), or only indirectly, through the release of further signaling molecules or neurotransmitters stimulating neurons (which were often suggested to be devoid of P2X7 receptors; Sim et al., 2004; Sperlágh et al., 2006). Our assumption that Bz-ATP activates P2X7 receptors at astrocytes was confirmed in the following series of experiments. In the whole-cell configuration of recording, the highly selective P2X7 receptor antagonist A-438079 (1, 10 μM) concentration–dependently inhibited the effect of Bz-ATP (300 μM) at astrocytes (Fig. 3Aa,b), and caused a maximal inhibition already at 1 μM in neurons (Fig. 3Ba,b). No further efforts were undertaken to characterize the P2X receptor type which mediated the Bz-ATP-sensitive, but A-438079-resistant part of the astrocytic current responses (10 μM A-438079; $18.0 \pm 6.5\%$; $n = 10$). A comparable residual current was also found in neurons (10 μM A-438079; $25.0 \pm 5.8\%$; $n = 10$). Bz-ATP is an agonist at most P2X receptor types (except P2X5 and −6), with particularly high potency at the P2X1,3 receptors (Jarvis and Khakh, 2009). However, P2X1 or P2X3 is unlikely to be involved as the Bz-ATP current did not exhibit desensitization, characteristic for these receptors.

However, Bz-ATP (300 μM) induced inward current in excised patches prepared from all astrocytes and neurons investigated. In four astrocytes out of a population of five, A-438079 (10 μM) inhibited the small Bz-ATP current to $48.1 \pm 11.4\%$ of its original height ($P < 0.05$); in the residual astrocyte there was no change of the current amplitude at all (100.8%; Fig. 3Ca,b). Further, in three neurons out of a population of six, A-438079 (10 μM) also depressed the tiny Bz-ATP current to $59.8 \pm 6.8\%$ of its original value ($P < 0.05\%$), whereas in the residual 3 neurons there was no statistically significant change ($122.0 \pm 15.0\%$; $P > 0.05$; Fig. 3Da,b). Thus, we confirmed that the majority of SG astrocytes possess P2X7 receptors and about one half of the SG neurons possess them as well.

The astrocyte shown in Fig. 3Ea was classified as one belonging to the transient class, based on its current–voltage characteristics. The blockade of NMDA (AP-5, 50 μM), AMPA (CNQX, 20 μM), $GABA_A$ (gabazine, 10 μM), and $glycine_A$ receptors (strychnine, 10 μM) almost abolished the Bz-ATP (300 μM)-induced currents in neurons, but did not alter the astrocytic responses (Fig. 3Eb,B,C). The coapplication of CNQX and AP-5 appeared to cause less inhibition (to $41.6 \pm 11.9\%$; $n = 6$) than that of CNQX, AP-5, gabazine, and sychnine (to $20.9 \pm 6.7\%$; $n = 10$; $P > 0.05$) although this difference did not reach the level of statistical significance. It can be suggested, however, that glutamate is released by the stimulation of astrocytic P2X7 receptors and that the Bz-ATP-induced currents at neurons are owing to the effect of this glutamate. The additional involvement of GABA or glycine could not be proven in spite of using the selective antagonists gabazine and strychnine.

Current Responses Induced by Bz-ATP in CA1 Neurons of the Hippocampus; Mediation of ATP Effects by Astrocytic P2X7 Receptors

In a previous study, we reported for astrocytes of the hippocampal oriens layer that P2X7 receptors mediate current responses in a low X^{2+} external medium (Oliveira et al., 2011). Now we found that neighboring CA1 neurons also respond to Bz-ATP with inward current in a low Ca^{2+}/no Mg^{2+} aCSF; such a change in the composition of the normal aCSF led to a sudden increase of the Bz-ATP (300 μM)

currents (Fig. 4Aa–c). A single neuron out of eight (Fig. 4Aa) was unresponsive to Bz-ATP in a normal aCSF, whereas the residual seven neurons exhibited a small current response under these conditions (Fig. 4Ab,c; 15.3 ± 4.2 pA; $n = 7$). It is noteworthy that CA1 pyramidal neurons of the hippocampus responded with very different current amplitudes to the same concentration of Bz-ATP when the scatter both within- and between-individual groups of experiments is taken into consideration (1,495.4 ± 995.3 pA, $n = 7$ in Fig. 4Ab; 2,438.9 ± 736.4 pA, $n = 5$ in Fig. 4Bb; 865.8 ± 267.1 pA, $n = 7$ in Fig. 4Cb).

Repetitive applications of Bz-ATP (300 μM) five times did not lead to a statistically significant reduction of the evoked current responses (Fig. 4Ca,b) although they had a tendency to decrease from S_2 to S_5. In consequence, we tested the effect of Bz-ATP (300 μM) before, during, and after superfusion with A-438079 (10 μM) (Fig. 4Da–b). The abolition of the agonist effect under these conditions unequivocally proves that P2X7 receptors are involved. It is noteworthy that Bz-ATP-induced currents in hippocampal stratum oriens astrocytes are also owing to P2X7 receptor stimulation as confirmed by investigating the interaction between Bz-ATP and A-438079 (10 μM) (Oliveira et al., 2011).

Potentiation of Neuronal Responses to Bz-ATP in the Spinal Cord SG but not the Hippocampal CA1 area by H_2O_2

The repetitive application of Bz-ATP (300 μM) to SG astrocytes induced stable current amplitudes with no change from the second to the fifth application (S_2-S_5; Fig. 5Aa,b). To avoid any possible variability of the first response, all responses were normalized with respect to the second Bz-ATP current. No comparable experiments were made to confirm the stability of the effect of Bz-ATP (300 μM) at neurons, but there was no reason to assume that repetitive application results in a change of amplitude (Fig. 3Ba). Then, Bz-ATP (300 μM) was superfused both in the absence and in the presence of H_2O_2 (100 μM) onto astrocytes (Fig. 5Ba,b) and neurons (Fig. 5Bc,d). H_2O_2 did not induce any current on its own, however, strongly potentiated the neuronal, but not astrocytic Bz-ATP currents to 259.6 ± 73.4% of their original amplitude ($n = 11$; $P < 0.05$). The antioxidant NAC (10 mM) also failed to act by itself; it decreased, however, the Bz-ATP current in neurons (to 51.6 ± 8.7%; $n = 8$; $P < 0.05$) but not astrocytes (Fig. 5Bb,d). These results as a whole suggest that exogenous and endogenous ROS facilitate P2X7 receptor-mediated effects only in neurons. Interestingly, catalase (1,000 U/mL), which degrades ROS, failed to alter the Bz-ATP current responses either in neurons or in astrocytes (Fig. 5Bb,d).

In analogy to the situation in the SG, a combination of AP-5 (50 μM) and CNQX (20 μM) strongly depressed the effect of Bz-ATP (300 μM) in the CA1 region (Fig. 5Ca,b). Already AP-5 caused slight inhibition, which was increased by the further addition of CNQX (to 14.2 ± 4.2%; $n = 6$). Eventually, AP-5, CNQX, and gabazine (10 μM) abolished the Bz-ATP-induced current (to 2.0 ± 0.5%; $n = 8$; $P < 0.05$ in comparison with AP-5 and CNQX only) (Fig. 5Cd), indicating that both glutamate and GABA are involved in the neuronal responses. However, in contrast to the reaction of SG neurons, the Bz-ATP (300 μM) effects in CA1 neurons were insensitive to H_2O_2 (100 μM) and astrocytic currents were even depressed by this agent (Fig. 5Da,b).

Measurement of the Bz-ATP-Induced Release of ROS from the Spinal Cord SG; Mediation by P2X7 Receptors

Superfusion of SG slices with BzATP (300 μM) for 2 min elicited a slow increase of their net ROS production, which was partly reversible upon washout (Fig. 6B). The maximal increase elicited by BzATP was 7.08 ± 1.99 μM ($n = 6$). Change of the perfusion solution with another one not containing Bz-ATP did not elicit any increase in net ROS production ($n = 3$; data not shown). Preperfusion with the selective P2X7 receptor antagonist A-438079 (10 μM) for 10 min *per se* failed to evoke detectable net ROS production (Fig. 6C; first half of the recording). The net ROS signal evoked by BzATP (300 μM) was significantly decreased in the presence of A-438079 (10 μM) (Fig. 6C; 1.30 ± 0.57 μM; $n = 5$; $P < 0.05$ from the effect of Bz-ATP alone).

Bz-ATP-Induced Currents in SG Astrocytes of Tg(GFAP/mRFP1) Mice

Eventually, a few transgenic Tg(GFAP/mRFP1) mice were used to prove that Bz-ATP (300 μM) induces current responses in GFAP-expressing astrocytes of the SG (Fig. 7). The selective P2X7 receptor antagonist A-438079 (10 μM) depressed the Bz-ATP current at S_3 to 12.2 ± 3.0% of its original amplitude ($n = 8$; $P < 0.05$). As the GFAP-expressing astrocytes were unequivocally identified on the basis of their red fluorescence, recording was without any doubt from this population of astroglia.

P2X7 Receptor Immunoreactivity at Microglia, but not at Astrocytes or Neurons of the SG

Most experiments were performed on 50-μm-thick SG slices, prepared from transcardially perfused rats, where P2X7 receptor immunoreactivity (IR) was colocalized with the microglial marker Iba1 (Fig. 8Ca–c), but not the astroglial markers GFAP or S100β (Fig. 8Aa–c,Ba–c), or the neuronal marker MAP2 (Fig. 8Da–c). We observed in all cases staining for the respective

cell-type marker, in the first column of Fig. 8a, staining for P2X7 antibodies in its second column (b) and the merged staining for both types of antibodies in its third column (c).

Immunohistochemistry in the stratum oriens of hippocampal slices resulted in similar results although the intensity of the staining was lower (data not shown). In histological specimens, microglia were in a resting, inactive state as proven by their numerous cellular processes (Fig. 8Ca). When the same investigations were made on 100-μm-thick SG slices superfused with aCSF for 2–3 h, thus, under conditions similar to those used for electrophysiological recordings, the quality of the immunohistochemistry pictures suffered from this treatments (Fig. 8Cci). The comparison of Fig. 8Cc with Cci shows that microglia was activated by the mechanical damage inflicted upon the living slices by the preparation procedure (round shape, no cellular processes). Microglia and astrocytes established often close spatial relationships.

The reason remains to be explained why P2X7 receptor IR was not found on astrocytes in spite of convincing evidence for the presence of functional P2X7 receptors on this cell type (for functional measurements in spinal cord slices of Tg(GFAP/mRFP1 mice, Fig. 7)). It is a well known fact that, for example, in the hippocampal CA1 area only ∼15% of the astrocytic population stains for GFAP-IR (Bushong et al., 2002). Therefore, we also used the glial marker S100β for being able to label a partially overlapping population of astrocytes. However, the P2X7-IR was absent in astrocytes stained either for GFAP or for S100β. Hence, we assume that the low density of such receptors might be a reason for this finding; large Bz-ATP/ATP-induced currents could be demonstrated only in a low X^{2+} external medium, which is known to greatly amplify P2X7 receptor function.

Discussion

The main finding of this study is that P2X7 receptors at SG astrocytes and neurons are functionally upregulated by a low Ca^{2+}/no Mg^{2+}-containing external medium; it is suggested that these receptors participate in the development of inflammatory and neuropathic pain. In fact, the use of genetically modified mice that lack the P2X7 receptor failed to develop pain after both inflammatory and neuropathic insults (Hughes et al., 2007). Furthermore, P2X7 receptor antagonists have been shown in animal studies to obliterate such types of chronic pain states (Andó et al., 2010; Carroll et al., 2009). The loss of P2X7 receptor antagonists to produce an antihyperalgesic effect in interleukin-1αβ knockout animals (Honore et al., 2009) confirmed that the release of interleukins mediated by P2X7 receptors is a key mechanism in inducing pain during inflammation. Eventually, in humans a genetic association between lower pain intensity and hypofunctional P2X7 receptors was reported to occur (Sorge et al., 2012).

Of course, the above findings do not differentiate between P2X7 receptors at peripheral immunocytes and their counterparts at microglia, astrocytes, and possibly neurons in the CNS. It has been reported that astrocyte-like satellite cells in sensory ganglia bear P2X7 receptors, whose activation may lead to the facilitation of pain-reactive P2X3 receptors at the primary sensory afferents (Burnstock et al., 2011; Chen et al., 2012). After lipopolysaccharide priming, P2X7 receptors release interleukin-1β in the spinal cord to cause mechanical hyperalgesia (Clark et al., 2010). These findings agree with the recently reported intimate interaction between astrocytes/microglia and neurons in various areas of the CNS. Especially, astrocytic and neuronal networks may communicate by gliotransmitters such as ATP and glutamate (Fellin et al., 2006), or cytokines, NO, and ROS (Safiulina et al., 2006).

In a very first series of experiments, we demonstrated by means of electrophysiological methods that SG astrocytes are endowed with functional P2X7 receptors, just like astrocytes in the cerebral cortex and hippocampal oriens layer (Leichsenring et al., 2013; Nörenberg et al., 2010; Oliveira et al., 2011). Although we did not perform this time a detailed pharmacological analysis, a few findings unequivocally prove that we deal with P2X7 receptors at SG astrocytes: (1) A low X^{2+} medium strongly accentuated the nucleotide-induced currents; (2) under these conditions, Bz-ATP was more potent than its mother compound ATP; and (3) the highly selective P2X7 receptor antagonist A-438079 almost abolished the effect of Bz-ATP (Anderson and Nedergaard, 2006; Sperlágh et al., 2006). In addition, SG neurons also responded to Bz-ATP and ATP, exhibiting some differences from their astrocytic effects. In the first line, the Bz-ATP-induced neuronal currents had a larger scatter around the mean than the astrocytic ones. In addition, ATP, in contrast to Bz-ATP caused only negligible current responses at SG neurons.

In view of the pertinent communication between astrocytes and neurons in various parts of the CNS, the question has arisen, whether the neuronal Bz-ATP/ATP effects are indirect, targeting originally astrocytes and transmitted to neurons by the release of a possible signaling molecule (Fellin et al., 2006; Safiulina et al., 2006). Specifically, P2X7 receptor activation at astroglia has been reported to release glutamate (Duan et al., 2003; Fellin et al., 2006), GABA (Wirkner et al., 2005), and ATP itself (Suadicani et al., 2006). By the use of selective antagonists for ionotropic glutamate (NMDA, AMPA) and GABA ($GABA_A$) receptors, we demonstrated that the neuronal Bz-ATP responses were strongly inhibited although usually not abolished. In contrast, the corresponding astroglial responses remained unchanged in the presence of these antagonists. In addition, excised patches from most SG astrocytes continued to respond to Bz-ATP in an A-438079 antagonizable manner. Surprisingly, excised patches prepared from a subpopulation of SG neurons also retained an

A-438079-antagonizable Bz-ATP effect. Excised patches are no longer in physical contact with the surrounding spinal cord tissue and therefore Bz-ATP currents should arise without contamination by signaling molecules of the neighboring cells. We conclude that P2X7 receptors are located primarily at SG astrocytes; the subsequently released glutamate and possibly GABA activates such receptors at SG neurons and induce inward currents. A minor contribution of neuronal P2X7 receptors situated at some SG neurons has been shown as well.

ROS, such as superoxide anion, hydrogen peroxide, and hydroxyl radicals are cytotoxic agents released, for example, by the oxidative burst of microglia in response to its activation processes. In addition, considerable evidence suggests that these species are able to act as cellular signaling molecules to regulate biological functions (Adler et al., 1999). In the CNS, H_2O_2 plays a role as an endogenous modulator of synaptic dopamine release (Chen et al., 2001), participates in the manifestation of synaptic plasticity (Knapp and Klann, 2002), and produces pain by reducing GABAergic inhibitory influence on SG neurons (Yowtak et al., 2011).

Hence, it was interesting to observe that H_2O_2 at a relatively low concentration of 100 μM markedly increased the Bz-ATP current at SG neurons, without causing any change in SG astrocytes. Correspondingly, when given alone, the antioxidant NAC depressed the neuronal but not astrocytic response to Bz-ATP. Thus, the inactivation of endogenous ROS by NAC or the application of exogenous H_2O_2 had opposite effects, supporting a possible reaction chain which involves the activation of P2X7 receptors at astrocytes, the subsequent production of ROS and finally the potentiation of the neuronal AMPA and/or NMDA receptor-mediated cationic fluxes. The following findings favor such a mode of action: (1) we found that Bz-ATP increases the production/release of ROS from SG slices, probably by stimulating astroglial P2X7 receptors. (2) ATP induced the generation of ROS in hippocampal astrocytes, albeit by $P2Y_1$ and not P2X7 receptor stimulation, and increased the frequency of $GABA_A$ spontaneous synaptic currents in CA3 pyramidal neurons (Safiulina et al., 2006). (3) ROS generated in Schwann cells contributed to the ATP-mediated negative feedback mechanism controlling the quantal secretion of acetylcholine from motor nerve terminals (Giniatullin et al., 2005). (4) Eventually, it has been concluded that ROS or reactive nitrogen species react with the lipoprotein cell membrane and may thereby indirectly alter the function of ionotropic transmitter receptors (Stojilkovic et al., 2013). A direct effect via the oxidation of critical cysteine residues (Cys-399 of the NR2A subunit, Choi and Lipton, 2000; Cys-430 of the P2X2 subunit; Coddou et al., 2009) at certain receptors of, for example, the NMDA- or P2X-types is also possible.

At an early developmental stage, ATP is definitely not the only, but probably the most powerful excitatory transmitter/signaling molecule in SG astrocytes. Astrocytes bear a number of pharmacological receptors including those for the excitatory amino acids glutamate (AMPA, NMDA) and the inhibitory amino acid GABA ($GABA_A$) (Lalo et al., 2011; Verkhratsky and Steinhäuser, 2000). We found that AMPA and NMDA had larger effects in neurons than in astrocytes, whereas the $GABA_A$ receptor agonist muscimol had comparable activity to stimulate its neuronal and astrocytic receptors at a fixed concentration of 100 μM. These findings are important in view of the well-known excitotoxicity of glutamate and ATP exerted by the stimulation of ionotropic AMPA/NMDA and P2X7 receptors, respectively. In fact, the significance of these receptor classes is increasingly recognized in stroke and neurodegenerative illnesses (Köles et al., 2011; Planells-Cases et al., 2006; Volonte et al., 2012). Similarly, they are involved in the spinal and supraspinal sensation of pain, especially in the case of neuronal damage (Bleakman et al., 2006; Burnstock et al., 2011; Planells-Cases et al., 2006).

In a low X^{2+} medium, CA1 hippocampal neurons also responded to Bz-ATP through P2X7 receptor activation, in agreement with the findings reported for astrocytes in the hippocampal oriens layer (Oliveira et al., 2011). However, in the hippocampus, CA1 neurons did not possess P2X7 receptors; glutamate and GABA of astrocytic origin appeared to mediate the inward current response to Bz-ATP. In addition, H_2O_2 failed to potentiate the Bz-ATP effect on neurons and even depressed it on astrocytes in this area of the brain. These are intriguing findings as ATP has been shown previously to release ROS from astrocytes in the hippocampus although by $P2Y_1$ rather than P2X7 receptor activation, and subsequently facilitated the spontaneous GABA release onto CA3 pyramidal neurons (Safiulina et al., 2006). Thus, either the astrocytic P2 receptor repertoire regulating ROS release varies in these two brain regions (P2X7 vs. $P2Y_1$), or the terminals of GABAergic interneurons innervating CA3 neurons possess ROS-sensitive $P2Y_1$ receptors, whereas CA1 neurons are devoid of P2X7 receptors, and their ionotropic glutamate receptors are not modulated by ROS.

Although the present evidence convincingly shows that P2X7 receptors are located at SG astrocytes and become unmasked in a low X^{2+} medium to operate as partners of SG neurons, the further participation of microglial P2X7 receptors as a third player on the stage cannot be excluded. The pathological function of microglia as a first defence barrier for all types of damage to the CNS is without question, but their roles in sensing and modulating neuronal activity as well as communicating with astrocytes has been only recently elucidated (Bezzi et al., 2001; Pascual et al., 2012). Thus, in response to various stimuli, microglia are activated and they

release small molecules such as nitric oxid, trophic factors, cytokines, and all types of neurotransmitters including ATP (Färber and Kettenmann, 2005). Hence, microglia endowed with P2X7 receptors may react to ATP and release interleukin-1β or tumor necrosis factor-α (Shieh et al., 2014) directly influencing SG neuronal activities; microglia could also release ATP (Imura et al., 2013), which stimulates astrocytic P2X7 receptors and thereby induces a glutamate/GABA receptor-mediated interaction with the SG neurons.

Conclusions

In conclusion, we describe a P2X7 receptor-triggered interaction between astrocytes and neurons in the SG of the spinal cord dorsal horn. Under the present *in vitro* conditions, this interaction operates only in a low Ca^{2+}/no Mg^{2+} medium. Such alterations in the ionic composition of the extracellular fluid may increase the susceptibility for neuronal discharges/seizures (Heinemann et al., 1992) known to depend on P2X7 receptors (Engel et al., 2012) and resembling the aetiology/pathogenesis of neuropathic pain. Hence, in accordance with the general view that P2X7 receptors, owing to their activation by large concentrations of endogenous ATP, function only under pathophysiological conditions (Sperlágh et al., 2006), in this study Bz-ATP/ATP caused rather small membrane currents in a normal external ionic milieu.

Author contributions

CF, TR, HF, BS, and PI conceived and designed the experiments. CF, TR, KR, EK, RDA, and LS performed the experiments. CF, KR, RA, EK, RDA, and LS analyzed the data. HF, BS, and PI Wrote the paper. TR, UK, HF, BS, and PI contributed financial support/reagents/materials/analysis tools. CF, EK, and PI drafted and edited the manuscript.

Acknowledgment

Grant sponsor: Deutsche Forschungsgemeinschaft; Grant numbers: RI 2092/1–2; IL 20/18-2; FR 1253/3-2; Grant sponsor: Hungarian Research and Development Fund; Grant number: NN107234; Grant sponsor: European Research Council; Grant number: 294313-SERRACO.

The authors thank Dr. Anna Leichsenring for help with some of the experiments as well as to Professor Nicholas Dale and the Sarissa Biomedical Co., for the supply and optimization of ROS biosensors. The generous gift of Tg(GFAP/mRFP1) mice by Dr. Petra G. Hirrlinger (Paul-Flechsig-Institut für Hirnforschung, University of Leipzig) is gratefully acknowledged.

References

Adler V, Yin Z, Tew KD, Ronai Z. 1999. Role of redox potential and reactive oxygen species in stress signaling. Oncogene 18:6104–6111.

Anderson CM, Nedergaard M. 2006. Emerging challenges of assigning P2X7 receptor function and immunoreactivity in neurons. Trends Neurosci 29:257–262.

Andó RD, Méhész B, Gyires K, Illes P, Sperlágh B. 2010. A comparative analysis of the activity of ligands acting at P2X and P2Y receptor subtypes in models of neuropathic, acute and inflammatory pain. Br J Pharmacol 159: 1106–1117.

Bezzi P, Domercq M, Brambilla L, Galli R, Schols D, De Clercq E, Vescovi A, Bagetta G, Kollias G, Meldolesi J, Volterra A. 2001. CXCR4-activated astrocyte glutamate release via TNFα: Amplification by microglia triggers neurotoxicity. Nat Neurosci 4:702–710.

Bleakman D, Alt A, Nisenbaum ES. 2006. Glutamate receptors and pain. Semin Cell Dev Biol 17:592–604.

Boucsein C, Kettenmann H, Nolte C. 2000. Electrophysiological properties of microglial cells in normal and pathologic rat brain slices. Eur J Neurosci 12: 2049–2058.

Brown AG. 1982. The dorsal horn of the spinal cord. Q J Exp Physiol 67:193–212.

Burnstock G, Wood JN. 1996. Purinergic receptors: Their role in nociception and primary afferent neurotransmission. Curr Opin Neurobiol 6:526–532.

Burnstock G, Krügel U, Abbracchio MP, Illes P. 2011. Purinergic signalling: From normal behaviour to pathological brain function. Prog Neurobiol 95: 229–274.

Bushong EA, Martone ME, Jones YZ, Ellisman MH. 2002. Protoplasmic astrocytes in CA1 stratum radiatum occupy separate anatomical domains. J Neurosci 22:183–192.

Carroll WA, Donnelly-Roberts D, Jarvis MF. 2009. Selective P2X7 receptor antagonists for chronic inflammation and pain. Purinergic Signal 5:63–73.

Chen BT, Avshalumov MV, Rice ME. 2001. H_2O_2 is a novel, endogenous modulator of synaptic dopamine release. J Neurophysiol 85:2468–2476.

Chen Y, Li G, Huang LY. 2012. P2X7 receptors in satellite glial cells mediate high functional expression of P2X3 receptors in immature dorsal root ganglion neurons. Mol Pain 8:9.

Choi YB, Lipton SA. 2000. Redox modulation of the NMDA receptor. Cell Mol Life Sci 57:1535–1541.

Clark AK, Staniland AA, Marchand F, Kaan TK, McMahon SB, Malcangio M. 2010. P2X7-dependent release of interleukin-1β and nociception in the spinal cord following lipopolysaccharide. J Neurosci 30:573–582.

Coddou C, Codocedo JF, Li S, Lillo JG, Racuna-Castillo C, Bull P, Stojilkovic SS, Huidobro-Toro JP. 2009. Reactive oxygen species potentiate the P2X2 receptor activity through intracellular Cys430. J Neurosci 29:12284–12291.

Duan S, Anderson CM, Keung EC, Chen Y, Chen Y, Swanson RA. 2003. P2X7 receptor-mediated release of excitatory amino acids from astrocytes. J Neurosci 23:1320–1328.

Engel T, Jimenez-Pacheco A, Miras-Portugal MT, Diaz-Hernandez M, Henshall DC. 2012. P2X7 receptor in epilepsy; role in pathophysiology and potential targeting for seizure control. Int J Physiol Pathophysiol Pharmacol 4:174–187.

Färber K, Kettenmann H. 2005. Physiology of microglial cells. Brain Res Brain Res Rev 48:133–143.

Fellin T, Sul JY, D'Ascenzo M, Takano H, Pascual O, Haydon PG. 2006. Bidirectional astrocyte-neuron communication: The many roles of glutamate and ATP. Novartis Found Symp 276:208–217.

Franke H, Günther A, Grosche J, Schmidt R, Rossner S, Reinhardt R, Faber-Zuschratter H, Schneider D, Illes P. 2004. P2X7 receptor expression after ischemia in the cerebral cortex of rats. J Neuropathol Exp Neurol 63:686–699.

Franke H, Verkhratsky A, Burnstock G, Illes P. 2012. Pathophysiology of astroglial purinergic signalling. Purinergic Signal 8:629–657.

Furue H, Katafuchi T, Yoshimura M. 2004. Sensory processing and functional reorganization of sensory transmission under pathological conditions in the spinal dorsal horn. Neurosci Res 48:361–368.

Giniatullin AR, Giniatullin AR, Grishin SN, Sharifullina ER, Petrov AM, Zefirov AL, Giniatullin RA. 2005. Reactive oxygen species contribute to the

presynaptic action of extracellular ATP at the frog neuromuscular junction. J Physiol 565:229–242.

Grudt TJ, Perl ER. 2002. Correlations between neuronal morphology and electrophysiological features in the rodent superficial dorsal horn. J Physiol 540:189–207.

Gu JG, MacDermott AB. 1997. Activation of ATP P2X receptors elicits glutamate release from sensory neuron synapses. Nature 389:749–753.

Gu JG, Gu JG, Heft MW. 2004. P2X receptor-mediated purinergic sensory pathways to the spinal cord dorsal horn. Purinergic Signal 1:11–16.

Heinemann U, Heinemann U, Albrecht D, Köhr G, Rausche G, Stabel J, Wisskirchen T. 1992. Low-Ca^{2+}-induced epileptiform activity in rat hippocampal slices. Epilepsy Res Suppl 8:147–155.

Heinrich A, Andó RD, Turi G, Rózsa B, Sperlágh B. 2012. K^+ depolarization evokes ATP, adenosine and glutamate release from glia in rat hippocampus: A microelectrode biosensor study. Br J Pharmacol 167:1003–1020.

Hirrlinger PG, Scheller A, Braun C, Quintela-Schneider M, Fuss B, Hirrlinger J, Kirchhoff F. 2005. Expression of reef coral fluorescent proteins in the central nervous system of transgenic mice. Mol Neurosci 30:291–303.

Honore P, Donnelly-Roberts D, Namovic M, Zhong C, Wade C, Chandran P, Zhu C, Carroll W, Perez-Medrano A, Iwakura Y, Jarvis MF. 2009. The antihyperalgesic activity of a selective P2X7 receptor antagonist, A-839977, is lost in IL-1$\alpha\beta$ knockout mice. Behav Brain Res 204:77–81.

Hughes JP, Hatcher JP, Chessell IP. 2007. The role of P2X7 in pain and inflammation. Purinergic Signal 3:163–169.

Illes P, Verkhratsky A, Burnstock G, Franke H. 2012. P2X receptors and their roles in astroglia in the central and peripheral nervous system. Neuroscientist 18:422–438.

Imura Y, Morizawa Y, Komatsu R, Shibata K, Shinozaki Y, Kasai H, Moriishi K, Moriyama Y, Koizumi S. 2013. Microglia release ATP by exocytosis. Glia 61: 1320–1330.

Jarvis MF, Khakh BS. 2009. ATP-gated P2X cation-channels. Neuropharmacology 56:208–215.

Knapp LT, Klann E. 2002. Potentiation of hippocampal synaptic transmission by superoxide requires the oxidative activation of protein kinase C. J Neurosci 22:674–683.

Köles L, Leichsenring A, Rubini P, Illes P. 2011. P2 receptor signaling in neurons and glial cells of the central nervous system. Adv Pharmacol 61:441–493.

Lalo U, Pankratov Y, Parpura V, Verkhratsky A. 2011. Ionotropic receptors in neuronal-astroglial signalling: What is the role of "excitable" molecules in non-excitable cells. Biochim Biophys Acta 1813:992–1002.

Lao LJ, Kawasaki Y, Yang K, Fujita T, Kumamoto E. 2004. Modulation by adenosine of Adelta and C primary-afferent glutamatergic transmission in adult rat substantia gelatinosa neurons. Neuroscience 125:221–231.

Landry M, Bouali-Benazzouz R, El Mestikawy S, Ravassard P, Nagy F. 2004. Expression of vesicular glutamate transporters in rat lumbar spinal cord, with a note on dorsal root ganglia. J Comp Neurol 468:380–394.

Leichsenring A, Riedel T, Qin Y, Rubini P, Illes P. 2013. Anoxic depolarization of hippocampal astrocytes: Possible modulation by P2X7 receptors. Neurochem Int 62:15–22.

Luo C, Kumamoto E, Furue H, Chen J, Yoshimura M. 2002. Nociceptin inhibits excitatory but not inhibitory transmission to substantia gelatinosa neurones of adult rat spinal cord. Neuroscience 109:349–358.

Nakatsuka T, Tsuzuki K, Ling JX, Sonobe H, Gu JG. 2003. Distinct roles of P2X receptors in modulating glutamate release at different primary sensory synapses in rat spinal cord. J Neurophysiol 89:3243–3252.

Nörenberg W, Schunk J, Fischer W, Sobottka H, Riedel T, Oliveira JF, Franke H, Illes P. 2010. Electrophysiological classification of P2X7 receptors in rat cultured neocortical astroglia. Br J Pharmacol 160:1941–1952.

Oliveira JF, Riedel T, Leichsenring A, Heine C, Franke H, Krügel U, Nörenberg W, Illes P. 2011. Rodent cortical astroglia express in situ functional P2X7 receptors sensing pathologically high ATP concentrations. Cereb Cortex 21:806–820.

Pascual O, Ben Achour S, Rostaing P, Triller A, Bessis A. 2012. Microglia activation triggers astrocyte-mediated modulation of excitatory neurotransmission. Proc Natl Acad Sci USA 109:E197–E205.

Planells-Cases R, Lerma J, Ferrer-Montiel A. 2006. Pharmacological intervention at ionotropic glutamate receptor complexes. Curr Pharm Des 12:3583–3596.

Safiulina VF, Afzalov R, Khiroug L, Cherubini E, Giniatullin R. 2006. Reactive oxygen species mediate the potentiating effects of ATP on GABAergic synaptic transmission in the immature hippocampus. J Biol Chem 281:23464–23470.

Santos SF, Melnick IV, Safronov BV. 2004. Selective postsynaptic inhibition of tonic-firing neurons in substantia gelatinosa by μ-opioid agonist. Anesthesiology 101:1177–1183.

Santos SF, Rebelo S, Derkach VA, Safronov BV. 2007. Excitatory interneurons dominate sensory processing in the spinal substantia gelatinosa of rat. J Physiol 581:241–254.

Shieh CH, Heinrich A, Serchov T, van Calker D, Biber K. 2014. P2X7-dependent, but differentially regulated release of IL-6, CCL2, and TNF-α in cultured mouse microglia. Glia 62:592–607.

Sim JA, Young MT, Sung HY, North RA, Surprenant A. 2004. Reanalysis of P2X7 receptor expression in rodent brain. J Neurosci 24:6307–6314.

Skaper SD, Debetto P, Giusti P. 2010. The P2X7 purinergic receptor: From physiology to neurological disorders. FASEB J 24:337–345.

Sorge RE, Trang T, Dorfman R, Smith SB, Beggs S, Ritchie J, Austin JS, Zaykin DV, Vander MH, Costigan M, Herbert TA, Yarkoni-Abitbul M, Tichauer D, Livneh J, Gershon E, Zheng M, Tan K, John SL, Slade GD, Jordan J, Woolf CJ, Peltz G, Maixner W, Diatchenko L, Seltzer Z, Salter MW, Mogil JS. 2012. Genetically determined P2X7 receptor pore formation regulates variability in chronic pain sensitivity. Nat Med 18:595–599.

Sperlágh B, Vizi ES, Wirkner K, Illes P. 2006. P2X7 receptors in the nervous system. Prog Neurobiol 78:327–346.

Stojilkovic SS, Leiva-Salcedo E, Rokic MB, Coddou C. 2013. Regulation of ATP-gated P2X channels: From redox signaling to interactions with other proteins. Antioxid Redox Signal (in press).

Suadicani SO, Brosnan CF, Scemes E. 2006. P2X7 receptors mediate ATP release and amplification of astrocytic intercellular Ca^{2+} signaling. J Neurosci 26:1378–1385.

Tsuda M, Inoue K, Salter MW. 2005. Neuropathic pain and spinal microglia: A big problem from molecules in "small" glia. Trends Neurosci 28:101–107.

Ulmann L, Levavasseur F, Avignone E, Peyroutou R, Hirbec H, Audinat E, Rassendren F. 2013. Involvement of P2X4 receptors in hippocampal microglial activation after status epilepticus. Glia 61:1306–1319.

Verkhratsky A, Krishtal OA, Burnstock G. 2009. Purinoceptors on neuroglia. Mol Neurobiol 39:190–208.

Verkhratsky A, Steinhäuser C. 2000. Ion channels in glial cells. Brain Res Brain Res Rev 32:380–412.

Volonte C, Apolloni S, Skaper SD, Burnstock G. 2012. P2X7 receptors: Channels, pores and more. CNS Neurol Disord Drug Targets 11:705–721.

Wirkner K, Günther A, Weber M, Guzman SJ, Krause T, Fuchs J, Köles L, Nörenberg W, Illes P. 2007a. Modulation of NMDA receptor current in layer V pyramidal neurons of the rat prefrontal cortex by P2Y receptor activation. Cereb Cortex 17:621–631.

Wirkner K, Köfalvi A, Fischer W, Günther A, Franke H, Gröger-Arndt H, Nörenberg W, Madarász E, Vizi ES, Schneider D, Sperlágh B, Illes P. 2005. Supersensitivity of P2X receptors in cerebrocortical cell cultures after in vitro ischemia. J Neurochem 95:1421–1437.

Wirkner K, Sperlágh B, Illes P. 2007b. P2X3 receptor involvement in pain states. Mol Neurobiol 36:165–183.

Yowtak J, Lee KY, Kim HY, Wang J, Kim HK, Chung K, Chung JM. 2011. Reactive oxygen species contribute to neuropathic pain by reducing spinal GABA release. Pain 152:844–852.